

Robust Dual Topological Character with Spin-Valley Polarization in a Monolayer of the Dirac Semimetal Na₃Bi

Chengwang Niu^{1,*}, Patrick M. Buhl¹, Gustav Bihlmayer¹, Daniel Wortmann¹, Ying Dai², Stefan Blügel¹, and Yuriy Mokrousov¹

¹*Peter Grünberg Institut and Institute for Advanced Simulation, Forschungszentrum Jülich and JARA, 52425 Jülich, Germany*

²*School of Physics, State Key Laboratory of Crystal Materials, Shandong University, 250100 Jinan, People's Republic of China*

Topological materials with both insulating and semimetal phases can be protected by crystalline (e.g. mirror) symmetry. The insulating phase, called topological crystalline insulator (TCI), has been intensively investigated and observed in three-dimensional materials. However, the predicted two-dimensional (2D) materials with TCI phase are explored much less than 3D TCIs and 2D topological insulator, while so far considered 2D TCIs almost exclusively possess a square lattice structure with the mirror Chern number $\mathcal{C}_M = -2$. Here, we predict theoretically that hexagonal monolayer of Dirac semimetal Na₃Bi is a 2D TCI with a mirror Chern number $\mathcal{C}_M = -1$. The large nontrivial gap of 0.31 eV is tunable and can be made much larger via strain engineering while the topological phases are robust against strain, indicating a high possibility for room-temperature observation of quantized conductance. In addition, a nonzero spin Chern number $\mathcal{C}_S = -1$ is obtained, indicating the coexistence of 2D topological insulator and 2D TCI, i.e. the dual topological character. Remarkably, a spin-valley polarization is revealed in Na₃Bi monolayer due to the breaking of crystal inversion symmetry. The dual topological character is further explicitly confirmed via unusual edge states' behavior under corresponding symmetry breaking.

The discovery of topological insulator (TI)^{1,2} has triggered an explosion of novel topologically nontrivial phases, such as the topological crystalline insulator (TCI), for which the role of the time-reversal symmetry is replaced by the crystal (mirror) symmetry³⁻⁵. The hallmark of a TCI, similar to a TI, is the presence of gapless surface/edge states with Dirac points inside of the insulating bulk energy gap. In presence of crystal mirror symmetry, the coexistence of TI and TCI phases has been predicted in three dimensions (3D) for Bi_{1-x}Sb_x⁶ and Bi chalcogenides⁷⁻⁹, and thus they exhibit a dual topological character (DTC). Recently, unusual topological surface states for a 3D DTC system have been observed experimentally^{8,9}. In the 2D case, graphene maybe a prototypical example of DTC^{10,11}. However, the extremely small band gap of graphene makes it very difficult to verify the DTC in this material experimentally¹². To date, the 2D TIs are identified experimentally in HgTe/CdTe¹³ and InAs/GaSb¹⁴ quantum wells at low temperatures, and a lot of 2D TIs with giant band gaps have been predicted to exist as a result of substrate interaction effect¹⁵, chemical functionalization¹⁶⁻²⁰, or global structure optimization²¹. In many cases the complex structures and the lack of mirror symmetry in such materials forbid the formation of a 2D TCI phase. On the other hand, 2D TCIs are so far limited to theoretical predictions that are mainly restricted to SnTe multilayers¹⁰, (Sn/Pb)(Se/Te) monolayers²²⁻²⁴, TI(S/Se) monolayers²⁵, and SnTe/NaCl quantum wells²⁶ with mirror Chern number $\mathcal{C}_M = -2$. The even number of band inversions leads to a vanishing \mathbb{Z}_2 invariant. Therefore, 2D TCIs with $\mathcal{C}_M = -2$ cannot be 2D TIs protected by the time reversal symmetry. Thus, for further investigation and applications of DTC in two dimensions, it is essential to extend the domain of candidate 2D TIs and TCIs both with respect to topological manifestations (i.e. different \mathcal{C}_M ²⁷) and material realisation.

For both 2D TIs and 2D TCIs, the spin-orbit coupling (SOC) is known to play a vital role. In addition, the SOC

together with inversion symmetry breaking can lead to coupled spin and valley physics, in which the new degree of freedom offers a promising route to the eventual realization of valleytronic devices^{28,29}. The spin-valley polarization has been observed experimentally in MoS₂ monolayer³⁰, which is a topologically trivial insulator. Therefore, a natural question arises as to whether the spin-valley polarization in nontrivial insulators, such as 2D TIs and 2D TCIs, is possible. Recently, thin films of the Dirac semimetal Na₃Bi^{31,32} have been fabricated by molecular beam epitaxy³³ and, therefore, in the present study, we take Na₃Bi as an example and propose the realization of the 2D DTC in a monolayer of Na₃Bi with a band gap of 0.31 eV, which is well above the energy scale of room temperature. The calculated spin Chern number $\mathcal{C}_S = -1$ and mirror Chern number $\mathcal{C}_M = -1$ confirm the 2D DTC phase directly. In addition, the spin-valley polarization due to the lack of the spatial inversion symmetry is investigated.

The density functional calculations are performed using the generalized gradient approximation (GGA) of Perdew-Burke-Ernzerhof (PBE)³⁴ for the exchange correlation potential as implemented in the FLEUR code³⁵ as well as in the Vienna *ab-initio* simulation package (VASP)^{36,37}. A 20 Å thick vacuum layer is used to avoid interactions between nearest slabs for VASP while the film calculations are carried out with the film version of the FLEUR code³⁸. SOC is included in the calculations self-consistently. The maximally localized Wannier functions (MLWFs) are constructed using the wannier90 code in conjunction with the FLEUR package.^{39,40}

Bulk Na₃Bi in hexagonal $P6_3/mmc$ structure is a three-dimensional (3D) counterpart of graphene, which hosts 3D Dirac points in its electronic structure and is called a topological Dirac semimetal^{31,32}. The bulk crystal structure consists of stacked triple layers along the z -direction. Each triple layer has four atoms which are one Bi in Wyckoff 2c position,

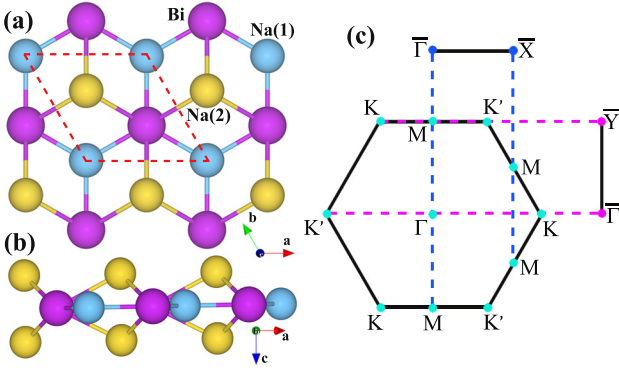


FIG. 1. (a) Top and (b) side view of honeycomb Na₃Bi monolayer, where the unit cell is indicated by the dashed lines. (c) The Brillouin zone of 2D Na₃Bi monolayer and the projected 1D Brillouin zones.

one Na(1) in 2b position, and two Na(2) in 4f position. In Figs. 1(a) and (b) the side and top view of the Na₃Bi triple layer are presented, with Bi and Na atoms forming the honeycomb lattice. Unlike in the bulk material, the inversion symmetry is broken in a Na₃Bi triple layer but the mirror symmetry $z \rightarrow -z$ is preserved, in exact analogy to a MoS₂ monolayer⁴¹. Hereafter, we call such a triple layer a Na₃Bi monolayer. To check its energetic stability, the formation energy is calculated by $E_f = E_{\text{Na}_3\text{Bi}} - 3\mu_{\text{Na}} - \mu_{\text{Bi}}$, where $E_{\text{Na}_3\text{Bi}}$ is the total energy of the Na₃Bi monolayer, μ_{Na} and μ_{Bi} are the chemical potentials of Na and Bi atoms, respectively. The calculated formation energy of -0.78 eV indicates that the Na₃Bi monolayer is energetically stable.

Figures 2(a) and (b) present the orbitally resolved band structures of Na₃Bi monolayer without and with SOC, respectively, that deliver preliminary insight into topological properties of the system. Due to the presence of time-reversal symmetry, the bands at valleys K and K' are energetically degenerate, and thus we only show the dispersion around K. In the absence of SOC, Bi-p_x and Bi-p_y orbitals contribute to the valence band maximum (VBM) while the conduction band minimum (CBM) is dominated by Bi-s orbitals with a direct band gap of 0.16 eV. Switching on SOC leads to an inversion of the VBM and the CBM, and an s-p band inversion occurs at Γ point. The insulating character is preserved with a band gap of 0.31 eV, indicating the feasibility of experimental observation of the 2D topological properties of this material at room temperature. To further confirm our results, the band structure is checked by using the more sophisticated Heyd-Scuseria-Ernzerhof hybrid functional method (HSE06)⁴². Similar to 1-T' MoS₂⁴³, the nontrivial phase has a larger band gap (~ 0.4 eV) when SOC is included.

The existence of the mirror symmetry $z \rightarrow -z$ (see Figs. 1(a) and (b)) for Na₃Bi monolayer promises the possibility of realizing the TCI that is characterized by the so-called mirror Chern number^{3,6}, which is defined as $C_M = (C_{+i} - C_{-i})/2$, where C_{+i} and C_{-i} are the Chern numbers for mirror eigenvalues $+i$ and $-i$,⁴⁴

$$C_{\pm i} = \frac{1}{2\pi} \sum_{n < E_F} \int_{BZ} \Omega_{\pm i}(\mathbf{k}) d^2k, \quad (1)$$

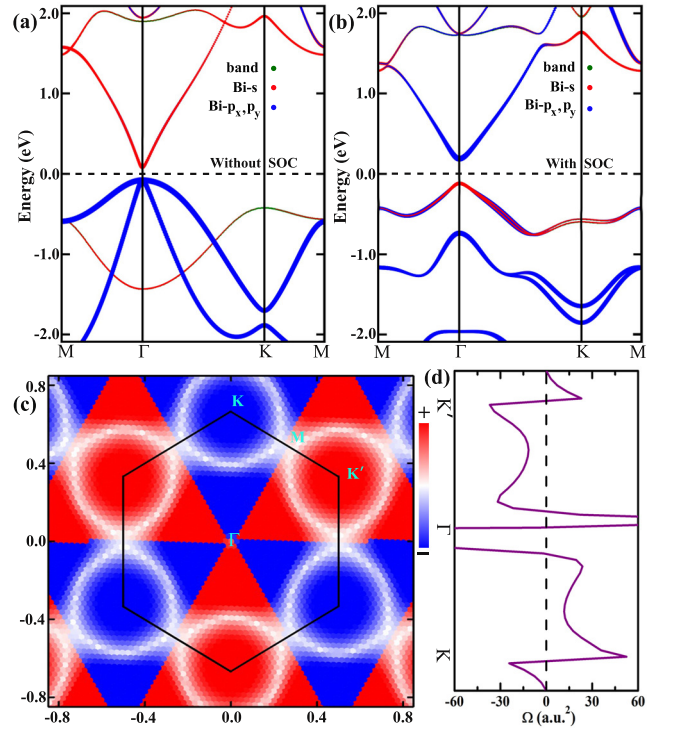


FIG. 2. Orbitaly-resolved band structures for Na₃Bi monolayer (a) without and (b) with SOC, weighted with the contribution of Bi-s and Bi-p_{x,y} states. The Fermi level is indicated with a dashed line. (c) Momentum-resolved polarization of spin perpendicular to the mirror plane for the highest occupied band. (d) Berry curvature distribution of the highest occupied bands in the K - Γ - K' direction.

and $\Omega_{\pm i}(\mathbf{k})$ is the Berry curvature of all occupied bands constructed from respective mirror projected states in the mirror plane, calculated according to

$$\Omega(\mathbf{k}) = -2\text{Im} \sum_{m \neq n} \frac{\langle \psi_{n\mathbf{k}} | v_x | \psi_{m\mathbf{k}} \rangle \langle \psi_{m\mathbf{k}} | v_y | \psi_{n\mathbf{k}} \rangle}{(\varepsilon_{m\mathbf{k}} - \varepsilon_{n\mathbf{k}})^2}, \quad (2)$$

where m, n are band indices, $\psi_{m/n\mathbf{k}}$ and $\varepsilon_{m/n\mathbf{k}}$ are the corresponding wavefunctions and eigenenergies of band m/n , respectively, and v_x/v_y are the velocity operators. The MLWFs are constructed to calculate the Berry curvature efficiently. With $z \rightarrow -z$ mirror symmetry, the calculated Chern numbers are respectively $C_{\pm i} = \mp 1$, leading to a mirror Chern number $C_M = -1$. This indicates that the Na₃Bi monolayer is a 2D TCI. Interestingly, the $C_M = -1$ case we consider here is topologically distinct from the previously reported 2D TCIs, such as (Sn/Pb)Te^{10,23,24} and TI(S/Se)²⁵ with $C_M = -2$.

Here, in Na₃Bi monolayer, band inversion occurs at Γ point, i.e., we acquire an odd number of band inversions. To identify the relationship between the 2D TI and the odd number of band inversions in Na₃Bi monolayer, we calculate the spin Chern number C_S ⁴⁵⁻⁴⁷ which can be directly related to the \mathbb{Z}_2 topological invariant of the system. C_S provides equivalent characterization to \mathbb{Z}_2 number in that for time-reversal symmetric and inversion symmetric systems the even values of C_S correspond to a topologically trivial insulator state, while

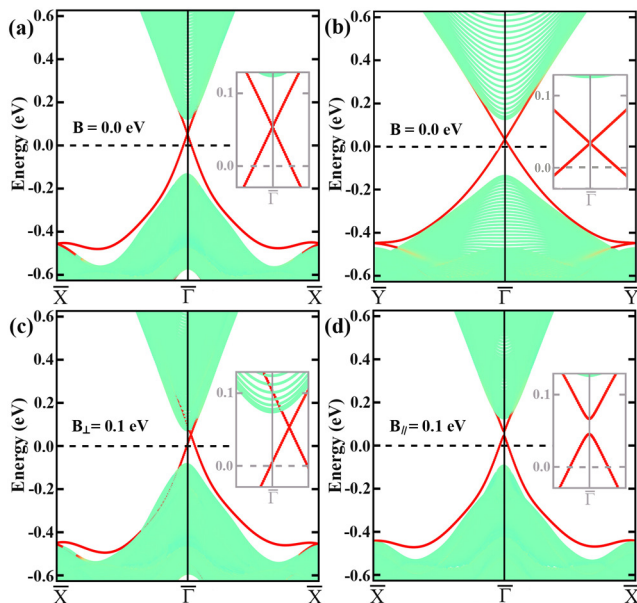


FIG. 3. Localization-resolved edge states of Na_3Bi monolayer for different configurations. (a) Bi-Na(1) termination without a magnetic field, (b) Bi-Na(1)-Na(2) termination without a magnetic field, (c) Bi-Na(1) termination a magnetic field perpendicular to the mirror plane, and (d) Bi-Na(1) termination with a magnetic field within the mirror plane. Insets show the corresponding zoom-in at the $\bar{\Gamma}$ point. Color from light green to red represents the weight of atoms located from middle to one edge of the ribbon structures.

odd values of \mathcal{C}_S indicate the emergence of a TI phase^{45–47}. The \mathcal{C}_S is given by the difference of the Chern numbers for the spin-up (\mathcal{C}_+) and spin-down (\mathcal{C}_-) projected manifolds, $\mathcal{C}_S = (\mathcal{C}_+ - \mathcal{C}_-)/2$ ⁴⁵. The σ_z matrix, $\langle \phi_{m\mathbf{k}} | \sigma_z | \phi_{n\mathbf{k}} \rangle$, is constructed and diagonalized to distinguish the spin-up and spin-down manifolds⁴⁷. The Chern number for each spin manifold is $\mathcal{C}_+ = -1$ and $\mathcal{C}_- = 1$, yielding the spin Chern number $\mathcal{C}_S = -1$. This clearly demonstrates the 2D TI nature of the Na_3Bi monolayer. Therefore, Na_3Bi monolayer exhibits the DTC with respect to the 2D TI and 2D TCI phases.

To further confirm the DTC, we investigate the edge states of 1D nanoribbons of Na_3Bi monolayer. The nonzero \mathcal{C}_M and/or \mathcal{C}_S should support the gapless edge states bridging the conduction and valence bands, which exhibit a band gap when both the time-reversal and mirror symmetries are broken. Based on a description in terms of MLWFs of the Na_3Bi monolayer, the tight-binding Hamiltonians of nanoribbons along two different directions with a width of 60 unit cells are constructed. The calculated band structures on one side of the ribbons are presented in Figs. 3(a) and (b), respectively. One can clearly see a pair of gapless edge states in the 2D gap. The Dirac point around $\bar{\Gamma}$ is a clear consequence of the non-trivial topological character of the system.

Generally, time-reversal symmetry breaking generates a gap in the surface/edge states of TIs^{1,2} while mirror symmetry breaking is indispensable for the formation of a band gap in the surface/edge states of TCIs³. One way to destroy these symmetries is to introduce the magnetism in the system. To

mimic a magnetic environment, we compute the matrix elements of the Pauli matrices σ_α ($\alpha = x, y, z$) in the basis of MLWFs, which allows us to consider the effect of an exchange field applied along different directions. For an exchange field perpendicular to the mirror plane, $H_{mag} = B_\perp \cdot \sigma_z$, the time-reversal symmetry is broken while the mirror symmetry is maintained. In this case, as shown in Fig. 3(c) for the Bi-Na(1) termination, the Dirac point moves slightly away from the $\bar{\Gamma}$ point, while a band gap does not open as a consequence of 2D TCI phase's survival. If the exchange field, on the other hand, is in the plane, $H_{mag} = B_\parallel \cdot \sigma_x$, both time-reversal and mirror symmetries are broken and the edge states become gapped (Fig. 3(d)). This behavior is reminiscent of that in $\text{Bi}_2(\text{Se/Te})_3$ ^{7,48}, but with different directions of an exchange field owing to a different sense of the mirror symmetry in these two compounds (B_z in the 3D TI corresponds to B_\parallel in the 2D TI)^{7,48}.

Exposing honeycomb lattices to inversion symmetry breaking provides a new, so-called valley, tunable degree of freedom in addition to spin and charge. The valley degree of freedom is receiving considerable attention these days due to potential application in valleytronics^{28,30}. To demonstrate the effect of the inversion symmetry breaking, we focus now on the spin-valley coupling of the Na_3Bi monolayer by considering the spin-polarization of occupied states in reciprocal space. Since the in-plane components of the spin polarization are vanishing due to the presence of mirror symmetry, in Fig. 2(c) we plot the momentum-resolved out-of-plane spin polarization of the highest occupied band. It is clearly visible that the highest occupied state exhibits the spin polarization which is of opposite sign at valleys K and K' . We further inspect the Berry curvature of the highest occupied band along the $K - \Gamma - K'$ path, plotted in Fig. 2(d). An odd behavior of the Berry curvature with respect to the valley agrees with the symmetry analysis in terms of time- and structural-inversion symmetry, similarly to the well-known case of spin-valley coupling in MoS_2 monolayer⁴⁹. Valley polarization that is coupled with spin will suppresses spin and valley relaxation and is promising to prepare the information carriers for the next-generation electronic and optoelectronic devices³⁰.

Having established our material's DTC, accompanied by a band gap of 0.31 eV (which is large enough for practical applications at room temperature), we finally test its stability. The phonon spectrum calculation shows imaginary frequencies around the M point, but not at the Γ point, indicating that the band inversion at this point is robust. We demonstrate this by investigating the band inversion under various strains as well as substrates⁵⁰. The magnitude of strain is described by the ratio a/a_0 , where " a_0 " and " a " denote the lattice parameters of the unstrained (5.31 Å) and strained systems, respectively. The results of the calculations shown in Fig. 4, indicate that the band gap of Na_3Bi monolayer can be significantly enhanced upon straining, similarly to the results reported previously^{18,25}. There is no band-gap closing-reopening process between the valence and conduction bands (ΔE_Γ and E_{gap}) in a large range of strain from -12% to 20% . The persistent band inversion indicates that the topological character of the system is robust against the substrate-imposed strain, which is

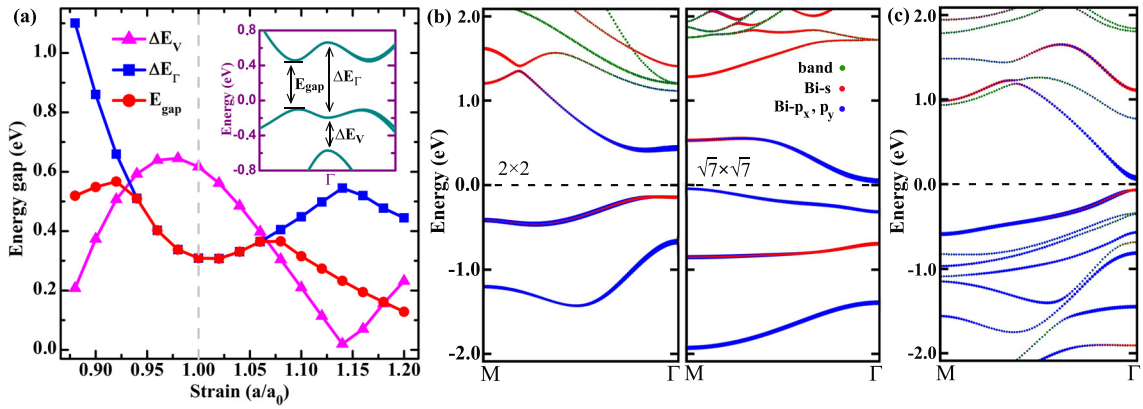


FIG. 4. (a) Variation of the energy gaps for Na_3Bi monolayer as a function of strain. The gaps (ΔE_Γ and E_{gap} in inset) between the valence and conduction bands remain while a strain-induced band inversion between the valence bands (ΔE_V in inset) occurs. (b) Orbitaly-resolved band structures for Na_3Bi monolayer sandwiched between a substrate of (b) BN with 2×2 and $\sqrt{7} \times \sqrt{7}$ supercells and (c) Na_3Sb , weighted with the contribution of Bi-s and Bi- p_x, p_y states. The DTC remains intact with corresponding substrates.

important for further experimental investigations and device applications due to the fact that a freestanding film is usually hard to grow. Figure 4(b) shows the calculated band structures of quantum well structures, that retain the mirror symmetry, with Na_3Bi monolayer sandwiched between 2×2 and $\sqrt{7} \times \sqrt{7}$ BN monolayers. As we can see, the energy gap at the M point changes much stronger than at Γ with the inverted band gap at the Γ point surviving in both cases (although a further band inversion occurs between valence bands for the $\sqrt{7} \times \sqrt{7}$ case, see also ΔE_V of Fig. 4(a)), which proves that DTC is preserved with respective substrate-induced strain of -6.2% and 19.7% . A weak interlayer interaction is expected between BN and Na_3Bi because of the large relaxed interlayer distances $\sim 4.0 \text{ \AA}$. We then consider a strong interlayer interaction via the topologically trivial substrate Na_3Sb that has the same crystal structure as Na_3Bi but creates -2% epitaxial strain. As shown in Fig. 4(c), the band inversion remains at the Γ point.

In summary, based on first-principles calculations, we revealed that the 2D TI and 2D TCI phases can coexist in Na_3Bi monolayer with a large band gap of 0.31 eV. Nonzero spin Chern number and mirror Chern number, as well as nontrivial topological edge states confirm the dual topological character clearly. As the mirror symmetry is preserved for an out-of-plane exchange field, the gapless edge states survive but move away from the time-reversal invariant momenta, while a gap opens for in-plane exchange fields. At last, strain engineering shows that the dual topological character in Na_3Bi monolayer is robust in a large range of strain in which the nontrivial band gap can be tuned efficiently.

This work was supported by the Priority Program 1666 of the German Research Foundation (DFG) and the Virtual Institute for Topological Insulators (VITI). We acknowledge computing time on the supercomputers JUQUEEN and JURECA at Jülich Supercomputing Centre and JARA-HPC of RWTH Aachen University.

* c.niu@fz-juelich.de

¹ M. Z. Hasan and C. L. Kane, Rev. Mod. Phys. **82**, 3045 (2010).
² X.-L. Qi and S.-C. Zhang, Rev. Mod. Phys. **83**, 1057 (2011).
³ L. Fu, Phys. Rev. Lett. **106**, 106802 (2011).
⁴ T. H. Hsieh, H. Lin, J. Liu, W. Duan, A. Bansil, and L. Fu, Nat. Commun. **3**, 982 (2012).
⁵ Y. Ando and L. Fu, Annu. Rev. Condens. Matter Phys. **6**, 361 (2015).
⁶ J. C. Y. Teo, L. Fu, and C. L. Kane, Phys. Rev. B **78**, 045426 (2008).
⁷ T. Rauch, M. Flieger, J. Henk, I. Mertig, and A. Ernst, Phys. Rev. Lett. **112**, 016802 (2014).
⁸ A. P. Weber, Q. D. Gibson, H. Ji, A. N. Caruso, A. V. Fedorov, R. J. Cava, and T. Valla, Phys. Rev. Lett. **114**, 256401 (2015).
⁹ M. Eschbach, M. Lanius, C. Niu, E. Młyniczak, P. Gospodarič, J. Kellner, P. Schüffelgen, M. Gehlmann, S. Döring, E. Neumann, M. Luysberg, G. Mussler, L. Plucinski, M. Morgenstern, D. Grützmacher, G. Bihlmayer, S. Blügel, and C. M. Schneider,

arXiv:1604.08886.

¹⁰ J. Liu, T. H. Hsieh, P. Wei, W. Duan, J. Moodera, and L. Fu, Nat. Mater. **13**, 178 (2014).
¹¹ C. L. Kane and E. J. Mele, Phys. Rev. Lett. **95**, 226801 (2005).
¹² Y. Yao, F. Ye, X.-L. Qi, S.-C. Zhang, and Z. Fang, Phys. Rev. B **75**, 041401 (2007).
¹³ M. König, S. Wiedmann, C. Brüne, A. Roth, H. Buhmann, L. Molenkamp, X.-L. Qi, and S.-C. Zhang, Science **318**, 766 (2007).
¹⁴ I. Knez, R. R. Du, and G. Sullivan, Phys. Rev. Lett. **107**, 136603 (2011).
¹⁵ M. Zhou, W. Ming, Z. Liu, Z. Wang, P. Li, and F. Liu, Proc. Natl. Acad. Sci. USA **111**, 14378 (2014).
¹⁶ Y. Xu, B. H. Yan, H. J. Zhang, J. Wang, G. Xu, P. Z. Tang, W. H. Duan, and S.-C. Zhang, Phys. Rev. Lett. **111**, 136804 (2013).
¹⁷ Z. Song, C.-C. Liu, J. Yang, J. Han, B. Fu, M. Ye, Y. Yang, Q. Niu, J. Lu, and Y. Yao, NPG Asia Mater. **6**, e147 (2014).
¹⁸ C. Niu, G. Bihlmayer, H. Zhang, D. Wortmann, S. Blügel, and Y. Mokrousov, Phys. Rev. B **91**, 041303(R) (2015).

- ¹⁹ L. Li, X. Zhang, X. Chen, and M. Zhao, *Nano. Lett.* **15**, 1296 (2015).
- ²⁰ C. P. Crisostomo, L.-Z. Yao, Z.-Q. Huang, C.-H. Hsu, F.-C. Chuang, H. Lin, M. A. Albao, and A. Bansil, *Nano. Lett.* **15**, 6568 (2015).
- ²¹ W. Luo and H. Xiang, *Nano. Lett.* **15**, 3230 (2015).
- ²² E. O. Wrasse and T. M. Schmidt, *Nano. Lett.* **14**, 5717 (2014).
- ²³ J. Liu, X. Qian, and L. Fu, *Nano. Lett.* **15**, 2657 (2015).
- ²⁴ C. Niu, P. M. Buhl, G. Bihlmayer, D. Wortmann, S. Blügel, and Y. Mokrousov, *Phys. Rev. B* **91**, 201401(R) (2015).
- ²⁵ C. Niu, P. M. Buhl, G. Bihlmayer, D. Wortmann, S. Blügel, and Y. Mokrousov, *Nano. Lett.* **15**, 6071 (2015).
- ²⁶ C. Niu, P. M. Buhl, G. Bihlmayer, D. Wortmann, S. Blügel, and Y. Mokrousov, *2D Mater.* **3**, 025037 (2016).
- ²⁷ R. Takahashi and S. Murakami, *Phys. Rev. Lett.* **107**, 166805 (2011).
- ²⁸ D. Xiao, W. Yao, and Q. Niu, *Phys. Rev. Lett.* **99**, 236809 (2007).
- ²⁹ A. Rycerz, J. Tworzydło, and C. W. J. Beenakker, *Nat. Phys.* **3**, 172 (2007).
- ³⁰ K. F. Mak, K. L. McGill, J. Park, and P. L. McEuen, *Science* **344**, 1489 (2014).
- ³¹ Z. Wang, Y. Sun, X.-Q. Chen, C. Franchini, G. Xu, H. Weng, X. Dai, and Z. Fang, *Phys. Rev. B* **85**, 195320 (2012).
- ³² Z. K. Liu, B. Zhou, Y. Zhang, Z. J. Wang, H. M. Weng, D. Prabhakaran, S.-K. Mo, Z. X. Shen, Z. Fang, X. Dai, Z. Hussain, and Y. L. Chen, *Science* **343**, 864 (2014).
- ³³ J. Hellerstedt, M. T. Edmonds, N. Ramakrishnan, C. Liu, B. Weber, A. Tadich, K. M. O'Donnell, S. Adam, and M. S. Fuhrer, *Nano Lett.* **16**, 3210 (2016).
- ³⁴ J. P. Perdew, K. Burke, and M. Ernzerhof, *Phys. Rev. Lett.* **77**, 3865 (1996).
- ³⁵ www.flapw.de.
- ³⁶ G. Kresse and J. Hafner, *Phys. Rev. B* **47**, 558 (1993).
- ³⁷ G. Kresse and J. Furthmüller, *Phys. Rev. B* **54**, 11169 (1996).
- ³⁸ H. Krakauer, M. Posternak, and A. J. Freeman, *Phys. Rev. B* **19**, 1706 (1979).
- ³⁹ A. A. Mostofi, J. R. Yates, Y. S. Lee, I. Souza, D. Vanderbilt, and N. Marzari, *Comput. Phys. Commun.* **178**, 685 (2008).
- ⁴⁰ F. Freimuth, Y. Mokrousov, D. Wortmann, S. Heinze, and S. Blügel, *Phys. Rev. B* **78**, 035120 (2008).
- ⁴¹ A. Splendiani, L. Sun, Y. Zhang, T. Li, J. Kim, C.-Y. Chim, G. Galli, and F. Wang, *Nano Lett.* **10**, 1271 (2010).
- ⁴² A. V. Krukau, O. A. Vydrov, A. F. Izmaylov, and G. E. Scuseria, *J. Chem. Phys.* **125**, 224106 (2006).
- ⁴³ X. Qian, J. Liu, L. Fu, and J. Li, *Science* **346**, 1344 (2014).
- ⁴⁴ Y. G. Yao, L. Kleinman, A. H. MacDonald, J. Sinova, T. Jungwirth, D.-S. Wang, E. Wang, and Q. Niu, *Phys. Rev. Lett.* **92**, 037204 (2004).
- ⁴⁵ Y. Yang, Z. Xu, L. Sheng, B. Wang, D. Y. Xing, and D. N. Sheng, *Phys. Rev. Lett.* **107**, 066602 (2011).
- ⁴⁶ E. Prodan, *Phys. Rev. B* **83**, 195119 (2011).
- ⁴⁷ H. Zhang, F. Freimuth, G. Bihlmayer, S. Blügel, and Y. Mokrousov, *Phys. Rev. B* **86**, 035104 (2012).
- ⁴⁸ L. A. Wray, S.-Y. Xu, Y. Xia, D. Hsieh, A. V. Fedorov, Y. S. Hor, R. J. Cava, A. Bansil, H. Lin, and M. Z. Hasan, *Nat. Phys.* **7**, 32 (2011).
- ⁴⁹ T. Cao, G. Wang, W. Han, H. Ye, C. Zhu, J. Shi, Q. Niu, P. Tan, E. Wang, B. Liu, and J. Feng, *Nat. Commun.* **3**, 887 (2012).
- ⁵⁰ K. Yang, W. Setyawan, S. Wang, M. B. Nardelli, and S. Curtarolo, *Nat. Mater.* **11**, 614 (2012).